JOURNAL OF CATALYSIS 120, 432–443 (1989)

CO Adsorption–Desorption Properties of Cation-Exchanged NaX Zeolite and Supported Ruthenium

N. M. GUPTA, V. S. KAMBLE, K. ANNAJI RAO, AND R. M. IYER

Chemistry Division, Bhabha Atomic Research Centre, Bombay 400 085, India

Received February 8, 1988; revised December 19, 1988

The binding states of carbon monoxide over cation-exchanged NaX zeolites and over corresponding Ru-containing samples have been investigated using thermal desorption spectroscopy. Exchange of sodium with cations such as Li^+, Ca^{2+}, Mg^{2+}, and La^{3+} gave rise to additional CO adsorption states, a higher isosteric heat of CO adsorption, an increased density of acid sites, and an increased amount of adsorbed CO, depending on the nature and ionic radius of the charge-balancing cation. The charge-balancing cations at the zeolite surface (e.g., Ca^{2+}, La^{3+}) function as additional CO adsorption sites in conjunction with surface acid centers (e.g., the Al^{3+} center) and metal sites. In addition to surface sites, CO is also found to be held in structural cavities and macropores of the zeolite matrix. The programmed heating of both the metal-free and Ru-containing zeolites subsequent to room temperature CO adsorption gave desorption peaks due to release of CO at temperatures less than ~500 K while the higher temperature peaks were constituted mainly of CO_2. Electron spectroscopy results have revealed that the exposure of these samples to CO and subsequent thermal treatment resulted in the formation of surface carbonaceous species. The nature of CO adsorption states giving rise to CO_2 formation is discussed.

INTRODUCTION

The zeolite-supported Group VIII metals have received considerable attention in recent years for use in CO methanation and Fischer–Tropsch synthesis (*1–14*). Catalytic activity, product selectivity, and adsorption stoichiometry of CO and H_2 have been found to be significantly affected by the chemical nature of the zeolite used. For instance, Oukaci *et al.* (*5, 15*) have shown that the substitution of Na^+ in RuNaY by Group I(A) cations affected the olefin-to-paraffin ratio in the CO hydrogenation process. Leith (*4*) has similarly observed that the olefin selectivity of zeolite-supported ruthenium in the hydrogenation of CO is enhanced with potassium- and cesium-exchanged zeolites.

It is widely accepted that metal–support interactions result in modifications of the electronic structure of the metal and are largely responsible for altered catalytic properties of supported catalysts. However, in the case of zeolite-supported catalysts, an important question that remains to be answered is whether zeolitic sites alter only the properties of the supported metal or whether they also are directly responsible for activating or adsorbing CO molecules.

In a previous paper (*16*) we have reported on the CO-binding states over NaX zeolites and RuNaX catalysts. Carbon monoxide has been found to be adsorbed in different pores and over zeolitic acid sites in addition to the Ru metal. The CO adsorbed over the acid sites was found to be converted to CO_2. It is well known that the exchange of sodium ions with smaller or larger cations produces a change in the electrostatic field inside the zeolite cavities and alters the sorption properties (*17–19*). The rate and mode of sorption of guest molecules would in turn affect the kinetics and product selectivity of a catalytic process involving the zeolitic support. In view of this a study on CO adsorption/desorption properties of cation-exchanged Na*X* zeolite and supported ruthenium catalysts was carried out. The effect on the binding states of carbon monoxide of substituting H^+, Li^+,

0021-9517/89 $3.00

Mg^{2+}, Ca^{2+}, and La^{3+} for Na^+ in NaX as investigated using thermal desorption spectroscopy (TDS) is reported here. Representative cations of varying valence states and ionic radii were so chosen that they were known to be inactive for CO dissociation/disproportionation reactions by themselves. Techniques of electron spectroscopy (XPS, AES) and X-ray diffraction (XRD) have been used to characterize the samples before and after CO exposure.

METHODS

Materials. A series of zeolite samples was prepared from NaX (from the Associated Cement Co., India) by substituting Li^+, H^+, Ca^{2+}, Mg^{2+}, and La^{3+} for sodium ions. For sample preparation a 60–80 mesh fraction of washed, and dried NaX was repeatedly contacted for different periods of time with aqueous solutions of nitrate or chloride of respective cations at pH 4–6 and at 350 K. The exchanged zeolites were washed repeatedly and dried at 385 K in air, followed by heating in a muffle furnace at 700 K for 18 h. The protonated (HX) samples were prepared by contacting NaX zeolites with aqueous ammonium nitrate solution and heating in H_2 at 625 K for 6 h before heat treatment at 700 K. The extent of exchange was determined by analysis of sodium and substituent cations using gravimetric and atomic absorption spectroscopy methods.

Ruthenium catalysts were prepared from the exchanged zeolites by depositing ~1.5 wt% Ru by an impregnation method using aqueous ruthenium chloride solution (*16*).

Thermal desorption spectroscopy. Thermal desorption spectra were recorded under dynamic He flow conditions using the instrumentation described elsewhere (*16*). Three-tenths gram of sample was used for each experiment and was given the following sequential treatments prior to CO exposures: H_2 (50 cm^3 min^{-1}, 625 K, 16 h), vacuum (10^{-1} Torr, 875 K, 30 min), and He (50 cm^3 min^{-1}, 875 K, 1 h). The sample was then cooled to 296 K under He flow. At this stage, about 10 carbon monoxide pulse injections (each containing 5.8 μmol CO diluted with 17 μmol He) were made into He carrier (20 ml min^{-1}) to completely saturate the sample with CO. The sample was thereafter equilibrated under He flow (50 ml min^{-1}) at 296 K for different periods of time ranging from 1 to 18 h. Gas desorption profiles were then recorded by heating the samples in helium at a linear rate of 30 K min^{-1} and detecting effluent gases by a gas chromatograph using a thermal conductivity detector. Qualitative analysis of the effluent gas composition was also carried out by mass spectrometry. Suitable purification treatments were given to He and H_2 gases to ensure that they were free from contaminants such as moisture and oxygen (*16*).

Characterization. The samples were characterized for their surface area (N_2 adsorption, BET method), intergranular pore size distribution (mercury porosimetry), crystal structure (powder XRD), and total number of acid centers (titration with *n*-butylamine). The samples for pore size evaluation by mercury porosimetry (Micromeritics 9200) were prepared by pressing ~1.5 g of material at 10,000 kg pressure. The heat of carbon monoxide adsorption over different samples was evaluated using gas chromatography. For this purpose, the CO retention volumes were determined at different bed temperatures for Na*X* and the isosteric heat of adsorption was evaluated using the expression (*20*)

$$\Delta H = R \cdot \frac{d \ln(V_g/T_c)}{d(1/T_c)},$$

where V_g is the retention volume per gram of sample and T_c is the sample bed temperature. Using the ΔH value thus obtained for NaX and the CO retention volumes over different exchanged samples, the comparative heats of adsorption data were calculated.

The surface characterization of different samples was carried out before and after CO exposure using X-ray photoelectron spectroscopy (XPS). A VG-ESCA-3 Mark

2 spectrometer employing Al$K\alpha$ radiation and oil diffusion pumps was used for this purpose at a base pressure of about 10^{-9} Torr in the main chamber. For these studies, the samples were pressed into 1-mm-thick pellets and were degassed for 6–10 h at 575 K under vacuum and then in the prechamber of the spectrometer for about 24 h at 300 K. The sputter-etched samples were exposed *in situ* to CO gas in the prechamber at 10^{-2} Torr and were heated at 600 K for 15 min. The survey and multiplex XPS profiles were recorded again after evacuating the samples first at 375 K for 30 min and then at 300 K. The charging shifts in the XPS peaks were calibrated with respect to the Cu $2p_{3/2}$ signal at 932.4 eV from the sample holder and the Al $2p$ (74.7 eV) or Si $2p$ (103.4 eV) signals from the zeolite. As adventitious carbon contamination was found to occur over any sample kept in the spectrometer, as is well known for systems using oil diffusion pumps, the samples were also analyzed by Auger electron spectroscopy (PHI 551 spectrometer with sputter ion pumps) before and after using them for CO TDS studies.

RESULTS

Sample Characteristics

The characteristics of different exchanged samples used in this study including that of Na*X* are given in Table 1. The surface area was found to decrease slightly on exchanging Na^+ with a larger cation and to increase with a smaller cation. Incorporation of Ru in the zeolites resulted in a slight decrease in the nitrogen absorption area, implying partial blockage of some of the pores.

Intragranular and intergranular pores (macropores) of similar sizes (in the range 0.025–40 μm) existed in all the pelletized samples, although small variations in pore size distribution were observed. Total macropore volume in these samples was in the range 0.14–0.15 ml g^{-1} and the average pore size was found to be around 0.1 μm. Although the larger pores would also exist in the samples packed in our catalyst column, they may not play a significant role in retention of CO molecules under the experimental conditions of this study.

TABLE 1

Physical Characteristics of Various Cation-Exchanged X Zeolites and Supported Ru (1.5%) Catalysts

Sample[a]	Cation radius (Å)	Surface area[b] (M^2 g^{-1} ±5%)		Total acidity[c] (Butylamine titre[d]) (μmol g^{-1})
		Metal-free	With Ru	
NaX	0.95	332	300	459
Li(83)X	0.60	350	310	526
H(6)X		—	—	611
H(70)X		260	245	577
Mg(62)X	0.66	354	295	580
Ca(80)X	0.99	310	280	782
La(75)X	1.05	300	278	832

[a] Figures in parentheses indicate % exchange.
[b] By BET method using N_2.
[c] Acid centers g^{-1} of zeolite.
[d] In H_0 range +6.8 to −1.5.

Relative intensities of powder XRD reflections from different samples are given in Table 2. Peaks with the same linewidths and at the same 2θ values were observed from NaX and exchanged samples (except HX), although their relative intensities were slightly different. In the protonated samples, a gradual loss of crystallinity with increasing protonation was revealed by a broad and intense background pattern and the absence of a number of XRD reflections (Table 2). At around 70% protonation, the zeolite structure collapsed completely, as already reported in the literature (*21*). Also, in the case of the La(75)X sample a partial amorphization was indicated by the presence of a broad background XRD pattern which is also reflected in the I/I_0 values given in Table 2 for this sample. XRD results indicated that, with the exception of protonated samples, no major lattice distortions are produced in the cation exchange process. Slight variations in the relative intensities of different Bragg reflections could

TABLE 2

Powder X-Ray Diffraction Data on Cation-Exchanged X Zeolites

2θ	I/I_0							
	NaX	Li(83)X	Mg(62)X	Ca(80)X	La(75)X	H(6)X	H(44)X	H(70)X
10	48.4	64	24.9	12.6	7.2	41.6	9.4	—
11.8	36.8	59	27.7	8.6	—	54	—	—
15.5	71	96	73.4	51.4	19.3	62.2	15.6	—
18.8	18.4	37.5	31.8	21.7	21.3	30	—	—
20.0	39.5	56.5	52	57	29	49.7	20.6	—
23.5	100	100	100	100	100	100	26.3	—
26.8	94.7	100	94.8	57	50.8	97.3	42	—
28.0	—	—	—	—	—	—	—	56.8
29.0	22	27.5	29	21.7	13.7	22.7	59.4	68.2
30.5	36.8	35	37.6	35.4	32	34.7	—	—
31.25	94.7	84	86.7	75.4	40.6	78.4	12.5	—
32.2	39.5	28	40.5	31.4	41.8	54	100	100
33.8	44.7	51	33.5	27	15.2	35	—	—
46.5	—	—	—	—	—	—	—	51.1

arise due to different types of charges associated with the exchanging cations.

XRD patterns from metal-free and corresponding ruthenium-containing samples and also from those samples which were used for CO adsorption/desorption were found to be almost identical, indicating again that these treatments do not lead to a significant lattice distortion.

CO Adsorption

Subsequent to the thermal pretreatments in H_2, vacuum, and He, as mentioned under Methods, when carbon monoxide pulses were injected over the catalyst bed at 298 K in a flowing helium carrier, a part of the CO from the first 3–4 pulses was adsorbed over the sample while the rest was eluted. The CO retention time measured by gas chromatography was found to be strongly dependent on the cation-exchanging sodium in NaX. In most of the exchanged samples the CO retention time was higher than that in NaX, the effect being most pronounced in the case of CaX. Ruthenium-containing exchanged zeolites showed weaker CO adsorption in terms of both the retention time and the amount of CO adsorbed compared to corresponding metal-free samples. The CO retention volumes for different samples are given in Table 3 along with the evaluated heats of CO adsorption.

THERMAL DESORPTION SPECTRA

Figure 1 shows the thermal desorption spectra from various cation-exchanged zeolite samples recorded 1 h after room tem-

TABLE 3

Gas Chromatographic Retention Volumes and Heat of CO Adsorption over Cation-Exchanged X Zeolites

Sample	CO retention volume (V_g)[a] (ml g^{-1})		Heat of CO adsorption (kJ mol^{-1})	
	Metal-free	With Ru	Metal-free	With Ru
NaX	57.8	56	14.9	14.5
Li(83)X	137.8	87.8	17.1	15.9
Mg(62)X	260.0	49.0	18.6	14.4
Ca(80)X	1038.0	604.4	22.1	20.7
La(75)X	70.0	60.0	15.3	14.9
H(6)X	76.7	92.2	15.4	15.9
H(44)X	147.8	—	17.16	—
H(70)X	36.7	33.3	13.64	13.4

[a] V_g = (retention time)(Carrier gas flow rate)/(sample mass).

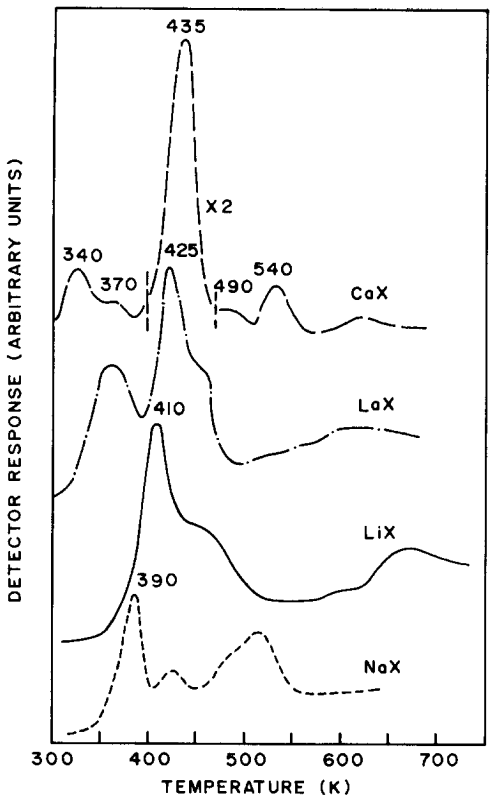

FIG. 1. TDS profiles from X zeolite samples containing different charge-balancing cations, recorded 1 h after CO exposure at 298 K.

perature adsorption of CO. The time interval between the CO exposure and the commencement of programmed heating affected the desorption profiles, as has been reported earlier (*16*). Figures 2a and 2b show the effect of the time interval in two typical cases of CaX and MgX samples. The data indicate that the number and temperature of different desorption peaks and also their relative intensities are significantly affected by the cation present in the zeolites. For instance, the intensity of a peak at ~420 K is at least two times greater in spectra from CaX and MgX compared to that from NaX (Figs. 1 and 2b). Also, in general, the temperature of this peak is found to be related with the acid site density (Table 1) and with the heat of CO adsorption (Table 3). The higher the heat of CO adsorption, the higher the temperature of this peak, the T_m for NaX, LiX, LaX, and CaX being 390, 410, 425, and 435 K, respectively. It is also of interest to note that in addition to different desorption peaks in the temperature range 390–550 K, the TDS profiles from exchanged zeolites exhibited additional peaks indicative of the generation of new CO adsorption states. These additional peaks were more prominent in the samples containing a cation with an ionic radius larger than that of sodium (e.g., Ca^{2+}, La^{3+}). Data of Fig. 2 show that with the increasing CO-injection/heating-commencement time interval, the intensity of peaks in the range 300–450 K was reduced while that of higher temperature peaks increased slightly, as was also observed in the earlier study using NaX (*16*).

Mass spectral analysis revealed that the effluent gases desorbed up to a temperature of about 475 K from different samples consisted mainly of carbon monoxide while at higher temperatures carbon dioxide was the principal component. Figure 3 gives typical qualitative data on desorbed gas composition from LaX and CaX samples.

Effect of Sample Crystallinity

To evaluate the role of zeolite pores in CO adsorption, it was desirable to study CO adsorption/desorption process over samples of varying crystallinity. As has been mentioned before, the HX zeolites lost crystallinity upon gradual increase in exchange level and at ~70% exchange complete structural collapse was indicated by XRD data. Using these protonated zeolites the CO TDS profiles as shown in Fig. 4 were obtained. It may be observed that the desorption peak intensity increased initially while in the sample containing higher H^+ concentration drastic reduction in the desorbed CO amount was observed and the T_m shifted to a lower value (Fig. 4). A similar CO adsorption/desorption behavior was observed with the cerium-exchanged samples which also lost their crystallinity in the course of sample preparation (*22*).

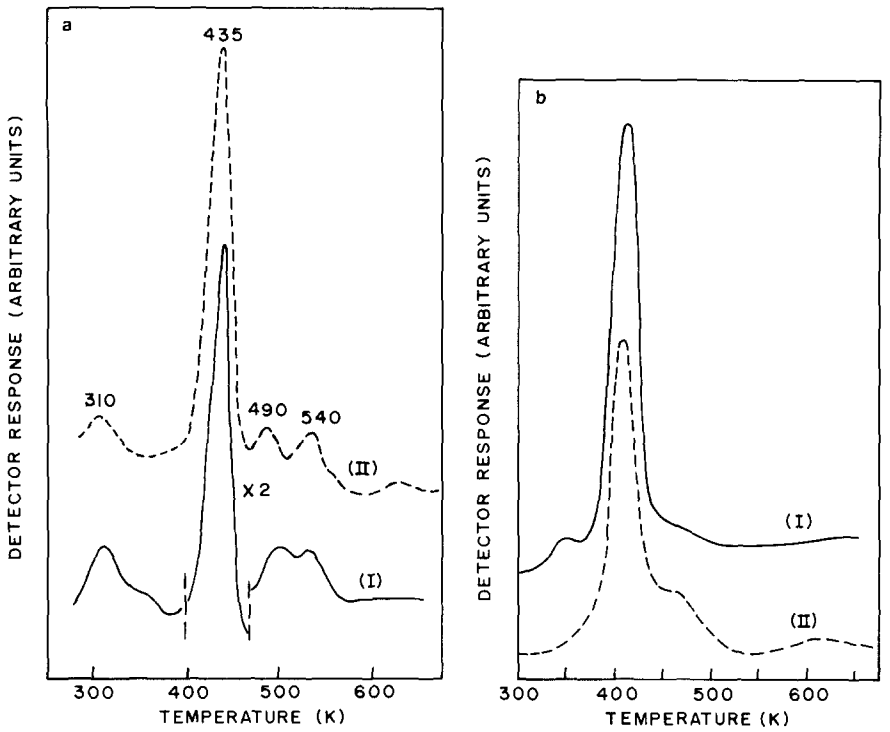

FIG. 2. TDS profiles from (a) CaX and (b) MgX zeolites obtained for (I) 1-h and (II) 16-h gap between CO exposure and commencement of heating cycle.

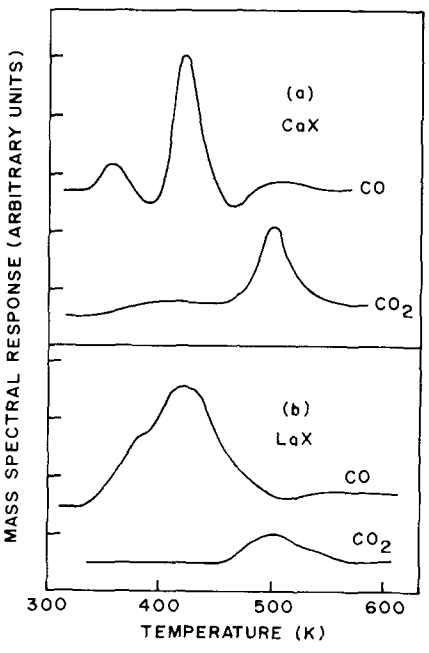

FIG. 3. CO and CO_2 desorption profiles from (a) CaX and (b) LaX zeolites, recorded 2 h after CO exposure.

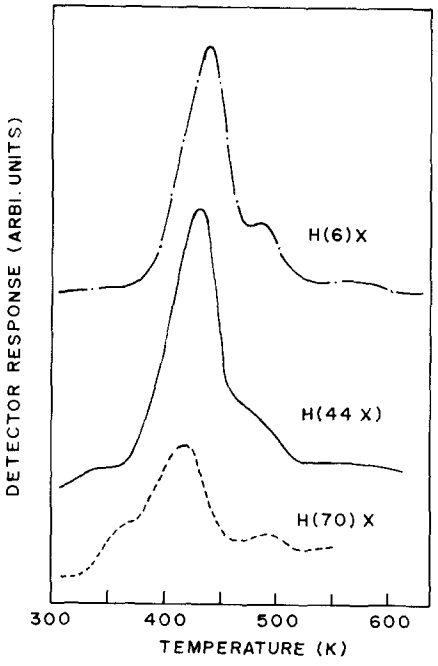

FIG. 4. TDS profiles from protonated X zeolites recorded 1 h after CO exposure.

Thermal Desorption Spectra from Ru-Containing Zeolites

Figure 5 shows thermal desorption profiles from different exchanged zeolites each containing ~1.5 wt% of Ru. A number of desorption peaks with maxima at around 325, 390, 445–450, 490, 530, 570, and 640 K were observed, the relative intensities of which depended on the cation present. A comparison of data in Figs. 1 and 5 reveals that the peaks in the range 300–500 K are common in TDS profiles from corresponding metal-free and Ru-containing samples, although their intensities were generally lower in the profiles from metal-containing zeolites. On the other hand, the TDS profiles from Ru/zeolite samples exhibited more intense high temperature peaks (T_m > 500 K).

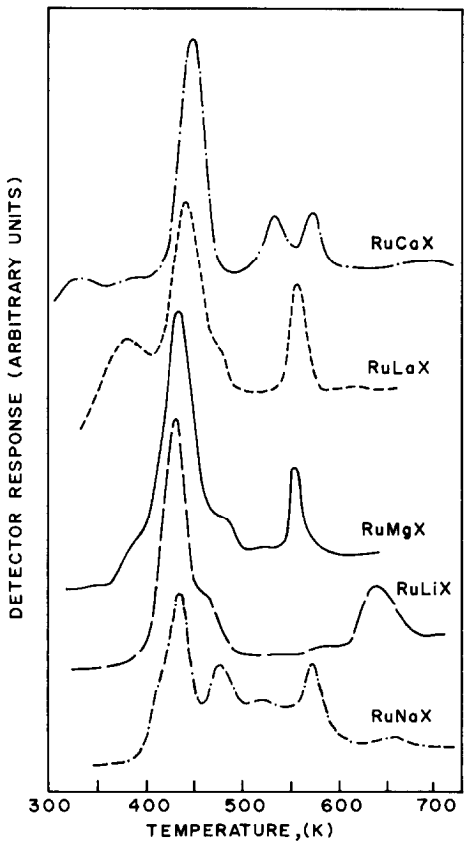

FIG. 5. TDS profiles from exchanged zeolite samples containing 1.5 wt% Ru, recorded 1 h after CO exposure.

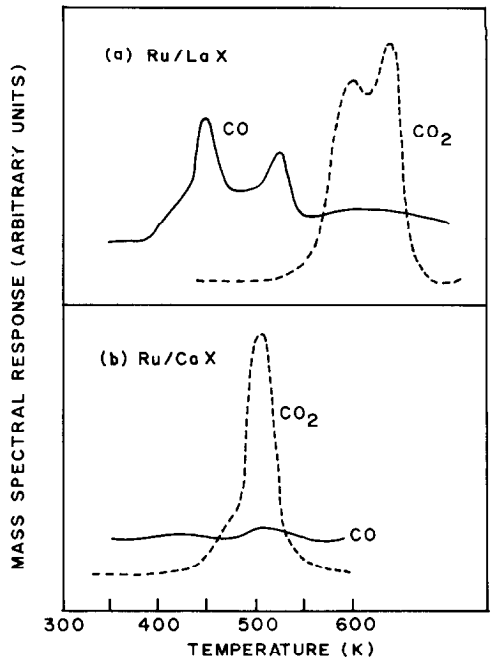

FIG. 6. CO and CO_2 desorption profiles from (a) RuLaX and (b) RuCaX samples, recorded 2 h after CO exposure.

Increasing the time gap between CO injection and thermal desorption had an effect on the TDS profiles similar to that observed in the case of metal-free zeolites; i.e., the peaks with T_m less than 550 K became less intense with increasing time gap while the high temperature peaks grew slightly in intensity.

Mass spectral analysis of thermally desorbed gases showed that, in general, the desorption peaks below 500 K were composed of CO while the higher temperature peaks were due to release of CO_2. In the exceptional case of RuCaX samples, the gas desorbed in the entire range of 300–700 K consisted mainly of CO_2. Figure 6 shows the composition of TDS profiles from Ru LaX and RuCaX samples.

Quantitative Evaluation of TDS Data

Although the quantitative evaluation of CO and CO_2 components in different de-

sorption spectra could not be made, the integrated area below a particular spectrum gave an estimate of the total amount of gases ($CO + CO_2$) desorbed from a particular sample. These data are given in Table 4 for both the metal-free and the corresponding ruthenium-containing samples. Comparison of these data reveals that the cation-exchanged zeolites had by and large a higher sorption capacity than NaX, the effect being most pronounced in CaX. It is also of interest to note that although the amount of gases held over NaX is considerably reduced with increasing CO-injection/heating-commencement interval, much larger proportions of $CO + CO_2$ were retained over exchanged zeolites even after a time lapse of about 16 h. For example, whereas in the case of NaX the amount of gas desorbed after a 16-h gap was about 45% of the amount desorbed after a 1-h gap, in the case of LiX, MgX, and CaX the corresponding figures were around 69, 80, and 70%. These observations clearly suggest that CO is more strongly bonded over exchanged samples than NaX, as is also reflected in the heat of adsorption data given in Table 3.

Data of Table 4 also indicate that while the amount of desorbed gas varied considerably with the nature of the cation present in zeolite X, in the case of Ru/zeolites the gas amounts in TDS profiles recorded in 1 h after CO exposure were almost independent of the cation.

TABLE 4

Effect of CO-Injection/Heating-Commencement Interval on the Amount of $CO + CO_2$ Eluted in Thermal Desorption Following Room Temperature CO Exposure over Exchanged Zeolite Samples and Supported Ru Catalysts

Sample	CO-injection/heating-interval (h)	
	1	16
	Amount of desorbed $CO + CO_2$ (μmol g^{-1} ±10%)	
NaX	4.4	2.0
LiX	6.1	4.2
MgX	7.3	6.4
GaX	9.7	6.8
LaX	6.8	4.2
RuNaX	6.7	3.7
RuLiX	6.5	6.3
RuMgX	6.0	—
RuCaX	6.1	5.2
RuLaX	6.4	—

XPS and AES Studies

In addition to the signals from framework elements, survey XPS spectra of different exchanged zeolites showed the presence of a small carbon signal with maximum at ~284 eV and a shoulder peak at 282 eV. Argon ion sputtering for about 2–4 min removed the surface carbon contamination. The C 1*s* XPS profiles from fresh and sputtered CaX samples are shown by curves a and b, respectively, in Fig. 7. When the sputtered samples were exposed to CO at 600 K, a large carbon signal at 284.2 ± 0.2 eV was observed. Curves c and d of Fig. 7 show C 1*s* spectra from CO-exposed CaX and LaX, respectively. The contamination due to residual spectrometer oil vapor gave a carbon signal at 282 ± 0.2 eV. Curve e of Fig. 7 shows the C 1*s* signal from contaminants deposited over a sample holder during overnight exposure in the spectrometer chamber.

An AES study has similarly confirmed that while the spectra from fresh NaX and exchanged zeolites showed negligible carbon signal, a large C KLL peak was observed in the spectra from samples used for recording TDS profiles.

Formation of surface carbon was also observed during CO exposure to Ru-containing samples. The XPS and AES studies and also the spectrochemical analyses have confirmed that no transition metal impurities (except about 100 ppm of Fe) were present in NaX or exchanged zeolites.

DISCUSSION

Synthetic zeolites have a well-defined pore structure depending upon the silica-to-

alumina ratio and the nature and distribution of the charge-balancing cations (*23, 24*). The catalytic properties of zeolites have their origin in surface sites identified generally as acid or basic sites (*24, 25*). A polycrystalline zeolite sample with a metal dispersed over its surface, as used in our study, would also have intergranular pores and may adsorb gas molecules over the following sites: (i) intracrystalline and intragranular zeolitic pores, (ii) Lewis acid sites, (iii) charge-balancing cations, and (iv) metal sites. The nature of the charge-balancing cation in zeolites is known to affect their catalytic properties by modifying one or more of the above sites (*23, 25*). It has been suggested that the cations may modify the electrostatic field in the zeolite pore system and give rise to new sites to bind guest molecules (*17, 18*). According to the "electrostatic theory" put forward by Rabo (*19, 26*), the field associated with cations results in polarization and increased concentration of reactant molecules in the zeolite pore system.

The salient results of the present study may be summed up as follows:

(a) data in Figs. 1 and 2 and in Table 4 show that the exchange of Na^+ in zeolite X with cations such as Li^+, Mg^{2+}, Ca^{2+}, and La^{3+} modifies CO-binding states, gives rise to new adsorption sites, and alters the amount of CO adsorbed;

(b) the amount of adsorbed CO was also related to the isosteric heat of CO adsorption and the density of acid sites over different exchanged samples;

(c) subsequent to CO adsorption at 298 K, the programmed heating gave rise to CO desorption in the temperature range 300–500 K while at higher temperatures mainly CO_2 was evolved;

(d) XPS and AES studies revealed that exposure of different zeolites to CO and subsequent heat treatment gave rise to the formation of carbonaceous species, the binding energy of the carbon signal (284.2 eV) corresponding with the value for graphitic carbon (*27*);

(e) the amount of CO adsorbed and the temperature of desorption peaks were also influenced by sample crystallinity.

Consideration of the activation energy values associated with different CO desorption peaks from NaX have led us to conclude that the peaks in the 400–500 K range resulted from the release of molecular CO from different zeolitic pores (*16*). In agreement with this view, the loss of crystallinity in H(70)X zeolite is reflected directly in the reduced amount of adsorbed CO (Fig. 4). On the other hand, although loss of crystallinity resulted in reduced CO uptake, a considerable amount of CO was still observed in H(70)X which was almost amorphous but had an acid strength comparable to that of LiX and MgX samples (Table 1). It can thus be suggested that both the surface sites and structural/intergranular pores play important and competitive roles in CO adsorption properties of zeolites.

The data of Figs. 1 and 2 show that the T_m of the most intense peak in NaX is 390 K which increases to 435 K in the case of CaX and MgX samples. It can therefore be concluded that the carbon monoxide molecules are more strongly bonded in zeolite pores when sodium ions are replaced with other cations, particularly second group elements. The alkaline earths are known to be preferentially localized in the small zeolite cavities of zeolites X and Y at the S_I, S_I', and S_{II}' positions (*28, 29*). These sites, however, would not be accessible to the CO molecules having a diameter of about 0.31 nm. Therefore, the cations at S_{II}' positions in α-cages may be identified as likely sites modifying adsorption properties of these zeolites.

The data in Figs. 1 and 2 also show that the additional CO desorption peaks are more prominent in those samples which are exchanged with cations greater in size than Na^+, for example, at 340, 370, and 620 K in the case of CaX and at 370 and 610 K in the case of LaX. The CaX and LaX samples also show a higher heat of CO adsorption (Table 3) and larger density of acid sites

(Table 1). It can thus be concluded that the presence of these cations not only modifies the field in the zeolitic pores but also gives rise to new CO-binding states.

Incorporation of additional adsorption sites in zeolites by exchanging cations has been suggested by several authors in recent years (*30, 31*). Michelena *et al.* (*32*) have shown that adsorption of CO and CO_2 over NaY zeolites is not controlled primarily by the pore volume but is dominated by forces between the adsorbate molecules and the adsorbent surface. A linear relationship was observed by these authors between the amount of adsorbed CO and the presence of accessible Ca^{2+} sites suggesting a strong Ca^{2+}–CO bonding. Connell and Dumesic (*33*) have shown that several cations doped in silica give rise to coordinatively unsaturated surface cations functioning as Lewis sites. Thus, it is now being realized that the promotional effect of alkali metals in the catalytic activity of transition metals for CO hydrogenation may not necessarily involve electron donation to the metal. The alkali metals may instead interact directly with CO, enhancing molecular adsorption (*34*). Our data support these views and confirm that the charge-balancing cations may themselves be responsible for the binding of CO molecules.

It is seen in Figs. 1 and 2 that the presence of charge-balancing cations not only induces low-temperature peaks originating from release of CO but also peaks at $T_m >$ 500 K which were due to desorption of CO_2 (Fig. 3). The study reported previously (*16*) has proposed that CO_2 formation in the interaction of CO over metal-free zeolites may involve the participation of Lewis acid sites (e.g., Al^{3+} ion with an empty *p* orbital). XPS (Fig. 7) and AES studies confirm that CO reacted over exchanged zeolites at elevated temperatures gives rise to significant amounts of surface carbon formation. It is therefore possible that both the compensating cations and Lewis sites may separately or jointly be involved in the CO adsorption process, giving rise to distinct binding states. ^{13}C NMR investigations have indeed shown that the CO adsorption over decationated NaX and NaY zeolites involves an interaction with Lewis acid sites (*35*).

The dehydroxylation of surface hydroxyl groups followed by carbon monoxide adsorption may be represented by the scheme given in Fig. 8. A threefold oxygen-coordinated aluminium atom as shown in structure (a) of Fig. 8 has been proposed by Uytterhoeven *et al.* (*36*) to be an adsorption center for guest molecules. The structure (b) in Fig. 8 could arise when the aluminum charge is balanced by electron donation from the carbon monoxide molecule, the charge-balancing cation acting independently as a CO adsorption site. Alternatively, a similar situation may also arise when a framework aluminum atom has a missing balancing cation due to a lattice imperfection. Recent NMR investigations (*37*) have, however, questioned the formation of a three-coordinated aluminum framework

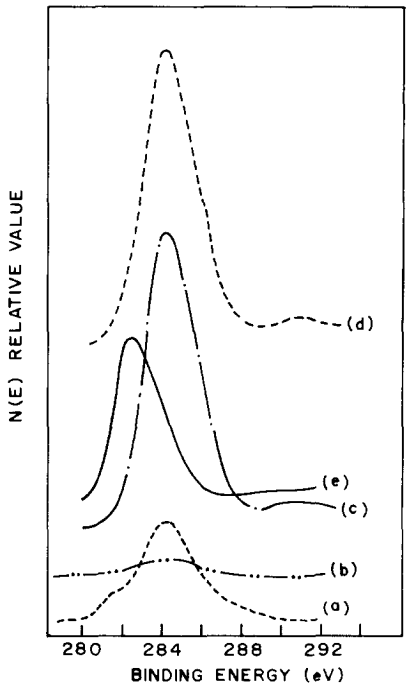

FIG. 7. XPS spectra of C 1*s* signal from fresh (a), sputter-cleaned (b), and CO-exposed CaX (c) samples. (d and e) C 1*s* signal from CO-exposed LaX and spectrometer contamination.

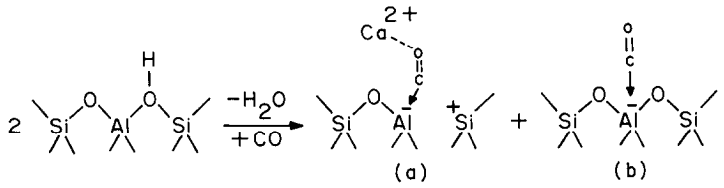

FIG. 8. Suggested modes of CO adsorption over dehydroxylated CaX zeolite.

(structure a, Fig. 8). X-ray and magic-angle spinning NMR spectroscopy studies (*38, 39*) have revealed that the dehydroxylation of decationated Y zeolites is accompanied by dealumination and formation of AlO^+ type species leached from the zeolite framework, and these species have been proposed to be true Lewis sites. If formed under the experimental conditions of our study, the Al–O-type segregated species may also act as adsorption sites where CO may be converted to CO_2 on thermal activation.

Dispersion of ruthenium metal would render a number of surface cations and zeolitic pores inaccessible to guest molecules as is revealed by reduction in N_2 adsorption area (Table 1). Therefore the metal is expected to reduce the intensity of different CO desorption peaks as is indeed observed in the data of Fig. 5 and in the almost similar CO + CO_2 yields obtained from different Ru-containing samples (Table 4). The additional high temperature peaks ($T_m > 600$ K) in desorption profiles from Ru-containing samples (Fig. 5) and the higher CO_2 yields from these samples during programmed heating (Fig. 6) are indicative of additional surface states produced by Ru metal where CO is disproportionated. The chemisorption and disproportionation of CO over Group VIII metals is a well known phenomenon (*34, 40*). Since the CO_2 formation increases when CO is adsorbed over zeolites for longer durations before thermal desorption (Fig. 2), it may be suggested that the reaction of CO molecules adsorbed at ruthenium or Lewis sites with the carbon monoxide occluded in zeolitic pores may provide an alternative route to CO_2 formation and surface carbon deposition.

CONCLUSIONS

The following conclusions may be drawn from the present study.

1. The amount of CO held in zeolitic pores and in intergranular macropores is significantly influenced by crystallinity and by the nature of the charge-balancing cation. The dispersion of ruthenium results in further modification of surface characteristics and CO adsorption properties of the zeolite.

2. The charge-balancing cations not only modify the field in the zeolitic pores but also interact directly with adsorbate CO molecules, giving rise to additional adsorption sites. These additional sites lead to increased zeolitic acid strength and greater heat of CO adsorption. The cation–CO bonding may also give rise to a promotional effect in the CO hydrogenation process, similar to the effect of alkali metals in the catalytic activity of transition metals.

3. The charge-balancing cations assist in CO dissociation over the zeolite surface in conjunction with Lewis sites and supported metal.

4. The distribution and relative abundance of different CO adsorption states are likely to affect the activity and selectivity of metal/zeolite catalysts for CO hydrogenation reactions.

ACKNOWLEDGMENTS

The authors thank Shri P. M. Raole of RSIC, Indian Institute of Technology, Bombay, for recording the

XPS data. Dr R. Bhat of Metallurgy Division helped in mercury porosimetry data, while the percentage of cations exchanged in our samples was evaluated in the Analytical Chemistry Division of our Center.

REFERENCES

1. Suib, S. L., McMahon, K. C., Tau, L. M., and Bennett, C. O., *J. Catal.* **89,** 20 (1984).
2. Scherzer, J., and Fort, D., *J. Catal.* **71,** 111 (1981).
3. Leith, I. R., *J. Chem. Soc., Chem. Commun.* **93** (1983).
4. Leith, I. R., *J. Catal.* **91,** 283 (1985).
5. Oukaci, R., Sayari, A., and Goodwin, J. G., Jr., *J. Catal.* **102,** 126 (1986).
6. Melson, G. A., Crawford, J. E., Crites, J. W., Mbadcam, K. J., Stencel, J. M., and Rao, V. U. S., Intrazeolite Chemistry (G. D. Stucky and F. G. Dwyer, Eds.), ACS Symp. Ser. Vol. 218, p. 397. Amer. Chem. Soc., Washington, DC, 1983.
7. Lin, T. A., Schwartz, L. H., and Butt, J. B., *J. Catal.* **97,** 177 (1986).
8. King, D. L., *J. Catal.* **51,** 386 (1978).
9. Chang, C. D., Lang, W. H., and Silvestri, A. J., *J. Catal.* **56,** 268 (1979).
10. Caesar, P. D., Brennan, J. A., Garwood, W. E., and Ciric, J., *J. Catal.* **56,** 274 (1979).
11. Elliott, D. J., and Lunsford, J. H., *J. Catal.* **57,** 11 (1979).
12. Chen, Y. W., Wang, H. T., and Goodwin, J. G., Jr., *J. Catal.* **83,** 415 (1983).
13. Chen, Y. W., Wang, H. T., and Goodwin, J. G., Jr., *J. Catal.* **85,** 499 (1984).
14. Jacobs, P. A., Verdonck, J., Nijs, R., and Uytterhoeven, J. B., *Adv. Chem. Ser.* **178,** 15 (1979).
15. Oukaci, R., Wu, J. C. S., and Goodwin, J. G., Jr., *J. Catal.* **107,** 471 (1987).
16. Kamble, V. S., Gupta, N. M., and Iyer, R. M., *J. Catal.* **113,** 398 (1988).
17. Jacobs, R. A., *in* "Carboniogenic Activity of Zeolites," p. 63. Elsevier, Amsterdam, 1977.
18. Bartholomeuf, D., *in* "Catalysis by Zeolites" (B. Imelik *et al.*, Eds.), p. 55. Elsevier, Amsterdam, 1980.
19. Rabo, J. A., *in* "Zeolite Chemistry and Catalysis" (J. A. Rabo, Ed.), ACS Monograph 171, p. 332. Amer. Chem. Soc., Washington, DC, 1976.
20. Habgood, H. W., *in* "Solid Gas Interface" (E. A. Flood, Ed.), Vol. 2, p. 611. Dekker, New York, 1967.
21. Rabo, J. A., *in* "Zeolites: Science and Technology" (F. R. Ribeiro *et al.*, Eds.), Ser. 80E, p. 302, NATO Adv. Study Inst., The Hague, 1984.
22. Kamble, V. S., Gupta, N. M., and Iyer, R. M., unpublished work.
23. Gates, B. C., Katzer, J. R., and Schuit, G. C. A., "Chemistry of Catalytic Processes," p. 49. McGraw–Hill, New York, 1979.
24. Anderson, J. R., "Structure of Metallic Catalysts," p. 74. Academic Press, London, 1975.
25. Wojciechowski, B. W., and Corma, A., "Catalytic Cracking: Catalysts, Chemistry and Kinetics," p. 59. Dekker, New York, 1986.
26. Rabo, J. A., *in* "Catalysis by Zeolites" (B. Imelik *et al.*, Eds.), p. 341. Elsevier, Amsterdam, 1980.
27. Wagner, C. D., Riggs, W. M., Davis, L. E., Moulder, J. F., and Muilenberg, G. E., Eds., "Handbook of X-Ray Photoelectron Spectroscopy," p. 38. Perkin–Elmer Corp., USA, 1979.
28. Haynes, H. W., *Catal. Rev. Sci. Eng.* **17,** 273 (1978).
29. Egerton, T. A., and Stone, F. S., *Trans. Faraday Soc.* **66,** 2364 (1970); **69,** 22 (1973).
30. Ward, J. W., *in* "Zeolite Chemistry and Catalysis" (J. A. Rabo, Ed.), ACS Monograph 171, p. 118. Amer. Chem. Soc., Washington, DC, 1976.
31. Flockhart, B. D., Megarry, M. C., and Pink, R. C., *Adv. Chem. Ser.* **121,** 509 (1973).
32. Michelena, J. A., Peeters, G., Vansant, E. F., and De Bievre, P., *in* Molecular Sieves II (J. R. Katzer, Ed.), ACS Symp. Ser. Vol. 40, p. 393. Amer. Chem. Soc., Washington, DC, 1977.
33. Connell, G., and Dumesic, J. A., *J. Catal.* **105,** 285 (1987).
34. Vannice, M. A., *in* "Catalysis, Science and Technology" (J. R. Anderson, M. Boudart, Eds.), Vol. 3, p. 190. Springer-Verlag, Berlin, 1982.
35. Michael, A., Meiler, W., Michel, D., and Pfeifer, H., *Chem. Phys. Lett.* **84,** 30 (1981).
36. Uytterhoeven, J. B., Christner, L. G., and Hall, W. K., *J. Chem. Phys.* **69,** 2177 (1965).
37. For review, see Thomas, J. M., and Klinowski, J., *in* "Advances in Catalysis" (D. D. Eley, H. Pine, and Paul B. Weisz, Eds.), Vol. 33, p. 199. Academic Press, New York, 1985.
38. Jacobs, P. A., and Beyer, H. K., *J. Phys. Chem.* **83,** 1174 (1979).
39. Freude, D., Frohlich, T., Hunger, M., Pfeifer, H., and Scheler, G., *Chem. Phys. Lett.* **98,** 263 (1983).
40. Gupta, N. M., Kamble, V. S., and Iyer, R. M., *J. Catal.* **60,** 57 (1979).